JCB Article

Ribonucleoprotein-dependent localization of the yeast class V myosin Myo4p

Claudia Kruse,[1] Andreas Jaedicke,[1] Joël Beaudouin,[2] Florian Böhl,[1] Dunja Ferring,[1] Thomas Güttler,[1] Jan Ellenberg,[2] and Ralf-Peter Jansen[1]

[1]Zentrum für Molekulare Biologie, Universität Heidelberg, D-69120 Heidelberg, Germany
[2]Gene Expression and Cell Biology/Biophysics Programs, European Molecular Biology Laboratory, D-69117 Heidelberg, Germany

Class V myosins are motor proteins with functions in vesicle transport, organelle segregation, and RNA localization. Although they have been extensively studied, only little is known about the regulation of their spatial distribution. Here we demonstrate that a GFP fusion protein of the budding yeast class V myosin Myo4p accumulates at the bud cortex and is a component of highly dynamic cortical particles. Bud-specific enrichment depends on Myo4p's association with its cargo, a ribonucleoprotein complex containing the RNA-binding protein She2p. Cortical accumulation of Myo4p at the bud tip can be explained by a transient retention mechanism that requires *SHE2* and, apparently, localized mRNAs bound to She2p. A mutant She2 protein that is unable to recognize its cognate target mRNA, *ASH1*, fails to localize Myo4p. Mutant She2p accumulates inside the nucleus, indicating that She2p shuttles between the nucleus and cytoplasm and is exported in an RNA-dependent manner. Consistently, inhibition of nuclear mRNA export results in nuclear accumulation of She2p and cytoplasmic Myo4p mislocalization. Loss of She2p can be complemented by direct targeting of a heterologous *lacZ* mRNA to a complex of Myo4p and its associated adaptor She3p, suggesting that She2p's function in Myo4p targeting is to link an mRNA to the motor complex.

Introduction

Cytoplasmic transport of organelles and other macromolecular complexes, such as ribonucleoprotein (RNP)* particles, depends on motor proteins that recognize their corresponding cargo and carry it along cytoskeletal actin filaments or microtubules to their target sites (Hirokawa, 1998; Mermall et al., 1998; Karcher et al., 2002). There are three types of cytoskeletal motor proteins: dyneins, which are minus end–directed microtubule motors; kinesins, which are mostly plus end–directed microtubule motors; and myosins, which are actin-dependent motors mostly moving toward the barbed (growing) ends of actin filaments (Titus and Gilbert, 1999). The function of motor proteins during transport must be regulated, which happens by multiple ways, including regulation of their ATPase activity, affinity to the cargo, or affinity to cytoskeletal filaments (for an overview see Reilein et al., 2001).

Among myosin motor proteins, class V myosins belong to the most widely distributed unconventional myosins and have been discovered in yeast, plants, invertebrates, and vertebrates (Reck-Peterson et al., 2000). They are multimeric proteins with several light chains and two heavy chains, each one with an NH_2-terminal motor domain that binds to actin filaments and generates force by ATP hydrolysis. A neck domain that contains up to six IQ motifs binds regulatory light chains such as calmodulin or calmodulin-like polypeptides (Boyne et al., 2000; Bähler and Rhoads, 2002). The tail domain contains stretches predicted to form coiled-coil structures necessary for homodimerization followed by a large globular domain required for organelle binding (Provance and Mercer, 1999; Reck-Peterson et al., 2000). Myo5a, a vertebrate class V myosin, has been shown to work as a processive motor and stay bound to actin filaments throughout the mechanochemical cycle (Mehta et al., 1999; Tanaka et al., 2002), but there is evidence that yeast class V myosins work as nonprocessive motors (Reck-Peterson et al., 2001).

The online version of this article includes supplemental material.

Address correspondence to Ralf-Peter Jansen, ZMBH, Universität Heidelberg, Im Neuenheimer Feld 282, D-69120 Heidelberg, Germany. Tel.: 49-6221-546869. Fax: 49-6221-545892.
E-mail: r.jansen@zmbh.uni-heidelberg.de

C. Kruse and A. Jaedicke contributed equally to this work.

C. Kruse's present address is Stiftung Caesar, Friedensplatz 16, 53111 Bonn, Germany.

F. Böhl's present address is Wellcome/CR UK Institute, Tennis Court Road, CB2 1QR Cambridge, UK.

*Abbreviations used in this paper: FLIP, fluorescence loss in photobleaching; RNP, ribonucleoprotein; wt, wild type.

Key words: myosin-V; RNA localization; FLIP; myosin regulation; *ASH1*

The *Saccharomyces cerevisiae* genome encodes heavy chains of two class V myosins, Myo2p and Myo4p. Myo2p is essential and directly involved in polarized transport of secretory vesicles (Johnston et al., 1991; Govindan et al., 1995; Pruyne et al., 1998; Schott et al., 1999, 2002), inheritance of the vacuole and Golgi apparatus (Catlett and Weisman, 1998; Catlett et al., 2000; Rossanese et al., 2001), and orientation of the mitotic spindle (Yin et al., 2000).

In contrast to Myo2p, the only function that has been assigned to Myo4p to date is mRNA localization (Reck-Peterson et al., 2000). Transport of at least two mRNAs, *ASH1* and *IST2*, to the bud tip depends on Myo4p (Long et al., 1997; Takizawa et al., 1997, 2000). *ASH1* encodes a transcriptional repressor that is essential for the regulation of asymmetric mating type switching, whereas *IST2* codes for a putative ion channel with unknown function (Bobola et al., 1996; Sil and Herskowitz, 1996; Takizawa et al., 2000). Both mRNAs associate with Myo4p via two additional proteins, She2p and She3p. She2p directly binds to *IST2* and *ASH1* mRNA in vivo and in vitro (Böhl et al., 2000; Long et al., 2000; Takizawa and Vale, 2000; Takizawa et al., 2000). She3p binds both to the coiled-coil region of Myo4p's tail domain and to She2p, and therefore serves as an adaptor between the class V myosin and the She2p–mRNA complex (Böhl et al., 2000).

Under steady-state conditions, both yeast class V myosins are found to accumulate at the tip of the growing bud. Localization of Myo2p depends on its functional motor domain, but at least a fraction of Myo2p can localize to the bud tip after disruption of the actin cytoskeleton (Ayscough et al., 1997). In addition, an overexpressed Myo2p tail domain partially localizes to the bud tip (Reck-Peterson et al., 1999), suggesting that Myo2p might become localized by active transport and tail-dependent anchoring. In the case of Myo4p, an isolated tail domain is not able to localize (unpublished data) and mutations in the heavy chain that interfere with localization have not yet been described. However, disruption of several *SHE* genes that, similar to *MYO4*, are required for mRNA localization lead to Myo4p mislocalization. Deletion of *SHE3* results in a diffuse cytoplasmic distribution of Myo4p, indicating a requirement for the adaptor She3p for Myo4p localization (Jansen et al., 1996; Münchow et al., 1999). Disruption of *SHE5/BNI1* leads to mislocalization of Myo4p to the presumptive cytokinesis site (Münchow et al., 1999). The effect of a deletion of *SHE2* on Myo4p's localization has so far been ambiguous. Whereas Myo4p is found in small buds of early S-phase *she2Δ* mutant cells (Jansen et al., 1996), mitotic cells lacking She2p fail to accumulate the myosin in large buds (Münchow et al., 1999).

Recent data suggest that kinesins might be steered to their proper target compartment by associated and/or cargo proteins (Setou et al., 2002), but it is unknown whether cargo molecules also influence targeting of class V myosins. Here we show that bud-specific accumulation of the motor protein Myo4p requires its association with an RNP complex and can be explained by a transient She2p-dependent retention mechanism. Bud enrichment of the motor requires either a complex containing She2p and localized mRNAs or direct binding of an mRNA to the myosin-associated adaptor She3p. Furthermore, we present evidence that She2p shuttles between the nucleus and cytoplasm and is exported from the nucleus in an mRNA-dependent manner.

Results

Localization of Myo4p depends on She3p and the RNA-binding protein She2p

To address the role of the RNA-binding protein She2p in myosin localization, we followed the localization of GFP-tagged Myo4p in wild-type (wt) and *she* mutant cells. Fusion of a single GFP protein to Myo4p did only result in barely detectable GFP signal although the fusion protein was expressed (unpublished data). We therefore constructed an *MYO4* allele with two GFPs at the COOH terminus by PCR-based epitope tagging (see Materials and methods). The resulting fusion protein (termed Myo4–GFP) is functional and targets *ASH1* mRNA to bud tips (Fig. S1, available online at http://www.jcb.org/cgi/content/full/jcb.200207101/DC1). Like myc-tagged versions (Jansen et al., 1996; Münchow et al., 1999), Myo4–GFP localized to the bud tip or bud cortex in wt cells (Fig. 1 A). It completely failed to localize in cells deleted for *SHE3*. A weak signal of Myo4–GFP was detected in small buds of *she2Δ* cells, but the myosin was not enriched in mid- to large-size buds (Fig. 1 A), indicating that She2p is required for an efficient enrichment of Myo4p at the bud tip. Similar results were obtained for a fusion protein of Myo4p tagged with six myc epitopes (Myo4p–myc; unpublished data). The observed differences in signal intensity were not due to reduced Myo4p levels in mutant cells because similar levels of an epitope-tagged Myo4p were present in wt, *she2Δ*, and *she3Δ* extracts (Fig. 1 B).

Because She2p binds localized mRNAs and links them with the Myo4p–She3p motor protein complex (Böhl et al., 2000; Long et al., 2000), we wondered if these mRNAs also influence Myo4p localization. To test for RNA dependence of Myo4p bud accumulation, we generated a double deletion mutant that lacks both described localized mRNAs, *IST2* and *ASH1* (Long et al., 1997; Takizawa et al., 1997, 2000). In contrast to *she2Δ* mutants, *ash1Δ ist2Δ* mutant cells showed a more efficient bud accumulation of Myo4–GFP (Fig. 1 A, bottom). Although this indicates that the two mRNAs are not essential for Myo4 localization, Myo4–GFP signals in the bud of *ash1Δ/ist2Δ* cells were often less intense. However, quantification of Myo4–GFP signals in mid-sized buds indicated that signal intensities within both populations of wt and double mutant cells showed too much variation in order to extract significant differences from the data sets of Myo4–GFP accumulation in wt versus double mutant cells (Fig. 1 C).

Nuclear mRNA export is required for Myo4p localization

The observation that deficiency of the mRNA-binding protein She2p, but not of two localized mRNAs, strongly influences accumulation of the Myo4p motor in the bud could be explained by an extra function of She2p in controlling

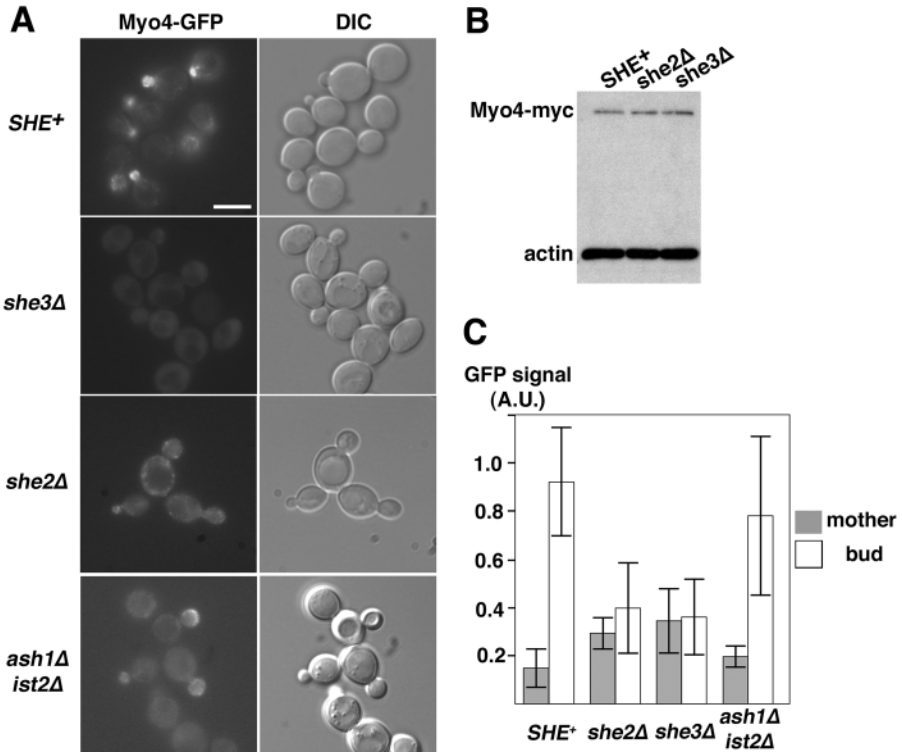

Figure 1. **Localization of Myo4–GFP depends on She2p and She3p.** (A, left) Myo4–GFP distribution in strains RJY1310 (wild type), RJY1304 (*she3Δ*), RJY1405 (*she2Δ*), and RJY1624 (*ash1Δ ist2Δ*). (A, right) DIC images of corresponding cells. Bar, 5 μm. (B) Western blot analysis against Myo4p–myc in *she2Δ* or *she3Δ* cells reveals that the stability of Myo4p is unchanged in *she* mutants. Western blot against actin served as a loading control. (C) Quantification of Myo4–GFP signal in bud and mother cells. GFP fluorescence of mid-sized buds (~2-μm diameter) and of an equivalent-sized area in mother cells was measured and is displayed as arbitrary units (A.U.). Error bars indicate the standard deviation of $n = 150$ measurements. Wt cells show on average a sixfold stronger signal in buds than mother cells, *ash1Δ/ist2Δ* cells a 4.5-fold and *she2Δ* cells a 1.3-fold stronger enrichment.

Myo4p localization. Alternatively, additional unknown localized mRNAs that also bind to She2p could compensate for the loss of *ASH1* and *IST2* (Takizawa et al., 2000). To interfere with the association of other localized mRNAs with Myo4p, we blocked nuclear mRNA export in a yeast mutant carrying a temperature-sensitive allele of the essential mRNA export factor *MEX67* (Segref et al., 1997). *mex67-5*^{ts} cells rapidly accumulate several mRNAs, including *ASH1*, in the nucleus at nonpermissive conditions (Hurt et al., 2000). Myo4–GFP localized to the bud tip in *mex67-5*^{ts} cells at 26°C, but the protein was completely delocalized after 30 min at 37°C (Fig. 2 A) when mRNA export had essentially ceased (Segref et al., 1997). In contrast, under identical conditions, Myo4–GFP localization remained unaltered in wt cells (*MEX67*$^{+}$), indicating that loss of myosin accumulation in the bud is not simply due to an unspecific temperature effect (Fig. 2 A, bottom). In addition, Myo2p, the second class V myosin in yeast, accumulated in buds under identical conditions (Fig. S2, available at http://www.jcb.org/cgi/content/full/jcb.200207101/DC1). In addition, polarized actin cables that are supposed to be required for directed myosin-based transport are still visible at a time when Myo4–GFP accumulation is completely lost (Fig. S2). Dependence of Myo4–GFP localization on mRNA export was further supported by the observation that Myo4–GFP localization resumes upon back-shift to the permissive temperature (Fig. 2 A, 37°C to 26°C) when mRNA export commences (Segref et al., 1997; unpublished data).

The observed localization defect could be due to a reduction of She2 or She3 protein levels during mRNA export block. However, the amounts of tagged She2p, She3p, or Myo4–GFP did not change at 37°C, even during a longer incubation, indicating that the half-life of these proteins is rather long (Fig. 2 B). We thus conclude from our data that nuclear export of mRNAs is essential for the localization of the cytoplasmic motor protein Myo4p.

The RNA-binding protein She2p shuttles between the nucleus and cytoplasm and is exported in an mRNA-dependent manner

Although She2p levels did not change during mRNA export block, the experiment did not address the question of whether the association of She2p with the Myo4–She3p complex remains unaffected. To investigate if She2p's localization is influenced by inhibition of mRNA export, we simultaneously determined the localization of She2p tagged with myc epitopes and an HA-tagged Myo4p in an *mex67-5* mutant (Fig. 3). Because efficient bud localization of She2p in our hands is only seen if localized mRNAs are overexpressed (Böhl et al., 2000; Takizawa and Vale, 2000), we investigated the effects of mRNA export on She2p and Myo4p in cells carrying *ASH1* under the control of the strong *GAL1* promoter. Under permissive conditions, Myo4p and She2p were found at the bud tip (Fig. 3, A and B). In contrast, in cells shifted to the nonpermissive temperature, a substantial fraction of She2p–myc accumulated in the nucleus (Fig. 3, E, E′, G, and G′). This suggests that She2p is able to enter the nucleus and that it is normally exported to the cytoplasm, possibly by an mRNA export–requiring mechanism. Cells with a nuclear She2p–myc signal failed to accumulate Myo4p–HA in the bud (Fig. 3, D and D′), whereas myosin localization was unaffected in the remaining cells lacking a strong nuclear signal of She2p–myc (unpublished data).

To address if RNA binding of She2p is essential for protein export to the cytoplasm, we generated a deletion mutant of She2p that does not bind to *ASH1* (see Materials

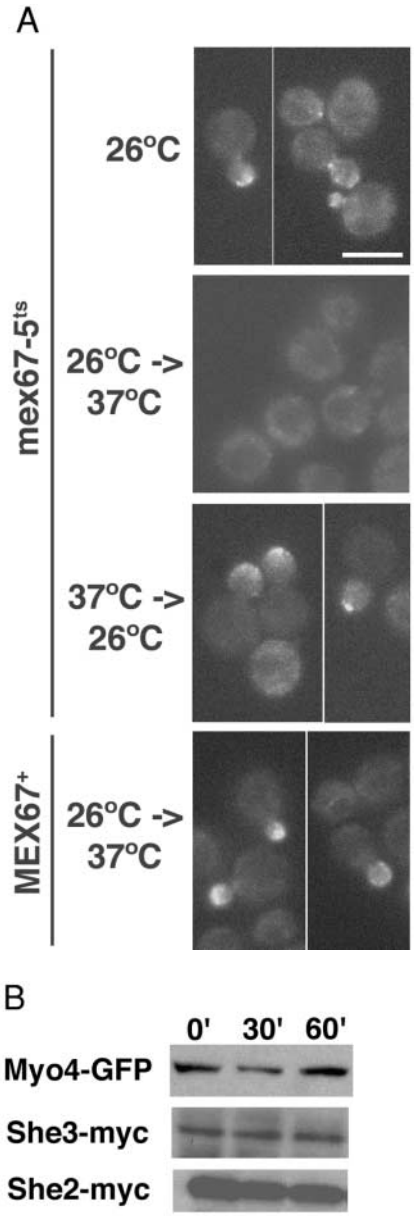

Figure 2. **Nuclear export of mRNA is required for Myo4–GFP localization.** (A) Images of representative Myo4–GFP cells from strains RJY1303 (*mex67–5*) or RJY1343 (*MEX67*). First panel, cells grown at 26°C; second and fourth panels, cells shifted for 30 min to 37°C; third panel, cells back-shifted for 20 min from 37°C to 26°C. Bar, 5 μm. (B) Western blot analysis against Myo4–GFP, She2p–myc3, and She3p–myc6 in *mex67-5* mutant. Myo4 and She protein levels do not change after a 60-min shift to 37°C and inhibition of nuclear mRNA export.

and methods). A truncated form of She2p lacking the first 70 amino acids (She2pΔN70) or the corresponding wt protein were expressed as myc-tagged versions in cells deleted for the endogenous *SHE2* gene. Wt and mutant proteins were immunoprecipitated with anti-myc antibodies and coprecipitating *ASH1* mRNA was detected by Northern dot blot (Fig. 4 A). Coprecipitation of *ASH1* mRNA was observed with wt She2p but not with a control protein, Cse1p. Deletion of the first 70 amino acids severely impaired She2p's competence to coprecipitate *ASH1* mRNA, indicating that the NH_2 terminus is essential for RNA binding.

We subsequently assessed the intracellular distribution of the mutant protein. In contrast to full-length She2p, which accumulates in the cytoplasm with only a little nuclear staining (Fig. 4 B, top), She2pΔN70 showed an increase in nuclear accumulation (Fig. 4 B, bottom). Similar to she2Δ mutants, yeast cells expressing She2pΔN70 failed to accumulate Myo4p–GFP at the bud tip (Fig. 4 C, bottom). Instead, cells showed diffuse staining in the mother cell with some filamentous staining of Myo4p–GFP. In summary, our data indicate that mRNA export is required for efficient cytoplasmic accumulation of She2p and that RNA binding of She2p is essential for its function in myosin localization.

RNA binding to the Myo4p–She3p complex is sufficient for Myo4–GFP localization to the bud

Is She2p essential for Myo4 localization or does it simply serve as linker between mRNA and the motor complex? To address this question, we used a system developed by Long et al. (2000). A fusion protein of She3p and the RNA-binding protein of phage MS2 was expressed in a strain lacking *SHE2*. This fusion protein recognizes RNAs containing MS2 binding sites and localizes a hybrid lacZ–MS2 mRNA to the bud tip (Long et al., 2000).

Localization of Myo4–GFP was not rescued by coexpression of the fusion protein with *lacZ* mRNA lacking MS2 binding sites (Fig. 5 A). Cells showed a diffuse signal of the GFP-tagged myosin. In contrast, Myo4–GFP accumulated in growing buds if She3p–MS2 was coexpressed with a hybrid of *lacZ* RNA and six, or one, MS2 binding sites (Fig. 5, B and C). In the case of a *lacZ* fusion with six MS2 binding sites, we observed bright dots at the cortex of the bud that sometimes showed movement along the cortex (unpublished data). Myo4–GFP signals at the bud tip were weaker and less concentrated when a lacZ–1xMS2 hybrid RNA was expressed, but accumulation at the bud was clearly visible. We conclude from these observations that direct targeting of a heterologous mRNA to the Myo4p–She3p motor protein complex is sufficient for Myo4p localization even in the absence of She2p, indicating that She2p itself is dispensable as long as mRNA associates with the Myo4p–She3p complex.

Cortical Myo4–GFP particles are highly dynamic structures

How might the association of an RNP influence the localization of the Myo4p motor? One possible explanation could be a change in the distribution kinetics of Myo4p of RNP-bound versus unbound myosin. We therefore followed the distribution of Myo4–GFP in wt and she2Δ cells using time-lapse confocal microscopy.

In wt cells, we observed bright dot-like signals in the bud that moved along the cortex (Fig. 6, top; see also Video 1, available online at http://www.jcb.org/cgi/content/full/jcb.200207101/DC1). Some bright dots appeared to split into smaller ones (Fig. 6, compare 10 and 15 s) and reassemble into a single bright dot (25 s), but the bright dot-like signals never left the cortex of the bud (Video 1). In contrast,

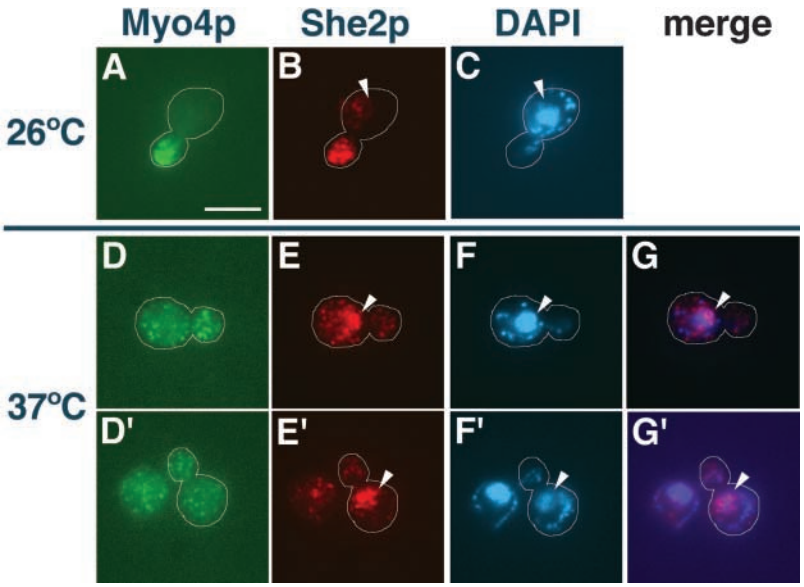

Figure 3. **She2p accumulates in nuclei upon inhibition of mRNA export.** (A–C) Strain RJY1613 (*mex67-5 MYO4–HA6 SHE2–myc9*) grown at 26°C. (D–G) Cells grown for 30 min at 37°C. (A, D, and D′) Anti-HA staining. (B, E, and E′) Anti-myc staining. (C, F, and F′) DNA staining by DAPI. (G and G′) Merge of E and F or E′ and F′, respectively. Arrowheads indicate the position of the nucleus and the white line indicates the cell boundary. Bar, 5 μm.

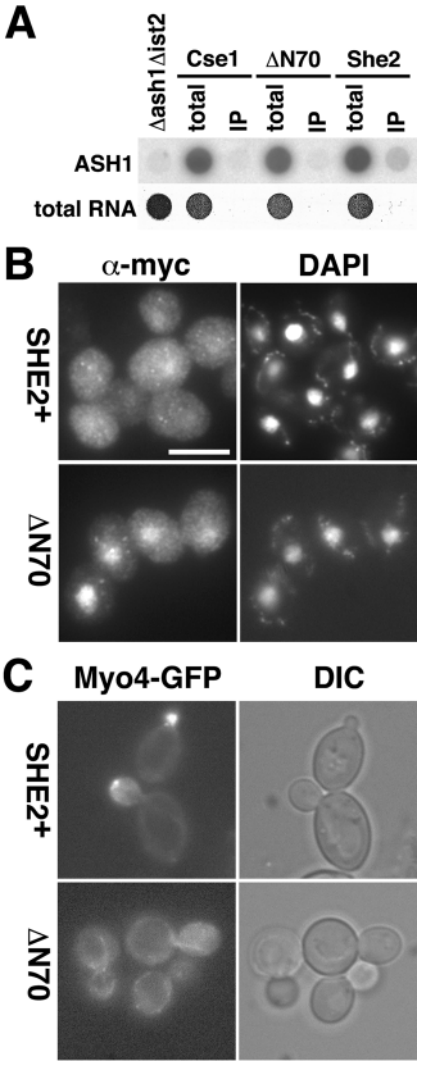

Figure 4. **The NH_2 terminus of She2p is required for RNA binding and efficient nuclear export of She2p.** (A, top) *ASH1* Northern dot blot of RNA isolated from cell extracts ("total") or RNA coprecipitated with myc-tagged Cse1p (strain RJY375), She2p (RJY1599), or She2pΔN70 (RJY1600). 1/18 of total RNA from an extract prepared from 8×10^9 cells or 1/2 of RNA isolated from an immunoprecipitation of myc-tagged proteins from 8×10^9 cells was applied to nylon membranes and probed for the presence of *ASH1* mRNA. Total RNA from a strain lacking *IST2* and *ASH1* mRNAs (RJY1004) was used as a control for unspecific binding of the probe. (A, bottom) Methylene blue staining of RNA. (B) She2pΔN70 localization differs from She2p localization. (B, left) Indirect immunofluorescence against myc-tagged She2p or She2pΔN70. (B, right) DNA staining with DAPI. Note that She2pΔN70–myc strongly accumulates in nuclei. Bar, 5 μm. (C) Myo4–GFP is mislocalized in an *she2ΔN70* mutant. (C, left) Myo4–GFP localization in strains RJY1526 (*SHE2*$^+$) and RJY1528 (*she2ΔN70*). (C, right) Corresponding DIC images.

Myo4–GFP in she2Δ cells was hardly detectable, consistent with our widefield fluorescence microscopy data (Fig. 6, bottom, insert). To follow Myo4–GFP movement over time, we therefore had to increase the gain of the detection system. Under these conditions, we observed smaller, less bright Myo4–GFP dots in the bud that quickly disassembled (Fig. 6, bottom, compare 5 with 10 s or 15 with 20 s; see also Video 2, available online at http://www.jcb.org/cgi/content/full/jcb.200207101/DC1) and reappeared again (compare 10 and 15 s). We also detected Myo4–GFP on filament-like structures in the mother cell that presumably were actin cables running from the mother cell into the bud (Fig. 6, bottom, 0 s). Such filamentous structures were also present in cells carrying an *she2ΔN70* mutation (Fig. 4 C, bottom) and could even be detected in wt cells, but were generally less strong than in the *she2* mutants (unpublished data).

We conclude that Myo4–GFP in the bud is a component of highly dynamic particles that stay associated with the bud cortex in wt cells. In *she2* mutant cells, the myosin is found in less bright particles in both mother and bud that break up and reform and that are not restricted to the cortex.

Myo4–GFP is retained only transiently in the bud, which depends on She2p

The observed effects of *she2* mutants on Myo4–GFP could be explained by a deficiency of myosin movement into the bud. However, low levels of bud-specific Myo4–GFP sig-

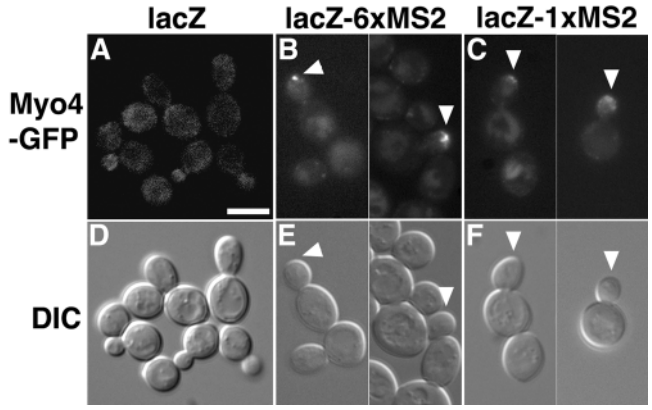

Figure 5. **RNA targeting to the Myo4p–She3p complex is sufficient for bud-specific myosin accumulation.** Localization of Myo4–GFP was determined in *she2Δ* cells expressing a fusion of She3p and MS2 coat protein (capable of binding to MS2 RNA stem loops) and *GAL1*-regulated *lacZ–ADHII3′UTR* (strain RJY1640), *lacZ–6xMS2–ADHII3′UTR* (RJY1641), or *lacZ–1xMS2–ADHII3′UTR* (RJY1813). Myo4–GFP localization was inspected after a 2-h induction with galactose. (Top) GFP signal. (Bottom) DIC images of corresponding cells. Note that Myo4–GFP is not accumulating in buds if lacZ mRNA lacks MS2 binding sites but is visible in single dots in buds of RJY1641 (six MS2 binding sites; arrows). Bar, 5 μm.

nal can be detected in *she2Δ* mutant cells, especially in small buds (Figs. 1 and 6). Alternatively, the observed variance could be explained by *SHE2*-dependent retention of Myo4p. To assess if Myo4–GFP can dynamically exchange between bud and mother cell and to measure its residence time in the bud, we performed fluorescence loss in photobleaching (FLIP) experiments on both wt and *she2Δ* cells expressing Myo4–GFP. FLIP is a technique used to analyze the rate limiting steps of exchange of fluorescently labeled protein between two compartments (mother and bud) in steady state (Lippincott-Schwartz et al., 2001). To achieve a pseudo steady-state situation, we chose cells ~1 h after budding with a bud diameter of 50% of the mother cell, a stage where intensity in the bud did not change significantly for at least 30 min (unpublished data). The mother cell was selectively photobleached every 5 s for a total of up to 10 min, and the depletion of fluorescence in the bud followed over time (Fig. 7). In *she2Δ* cells, where no strong enrichment of Myo4–GFP in the bud over the mother could be detected, the bud lost fluorescence rapidly and completely, with kinetics only slightly slower compared with the directly photobleached mother cell (Fig. 7 A). This, and the fact that shorter bleach intervals did not lead to a faster depletion of bud fluorescence (unpublished data), strongly argued that the depletion of Myo4–GFP was only limited by the exchange between bud and mother. Wt cells that displayed a more than threefold higher concentration of Myo4–GFP in the bud showed a slower depletion of bud fluorescence under identical conditions, but eventually could also be depleted completely during a 10-min FLIP experiment (Fig. 7 B).

To determine the characteristics of a retaining interaction that could lead to the concentration of Myo4–GFP in wt cells, we analyzed the depletion kinetics with a computer simulation. The simulation assumed two compartments in steady state, bud and mother, that can exchange Myo4p by diffusion. In addition, the simulation assumed that in wt cells, a fraction of Myo4p in the bud compartment was bound to a hypothetical receptor, whereas in *she2Δ* cells, the entire pool in the bud was assumed to be free. The bound pool in wt buds can only exchange with the mother compartment once it has dissociated from the binding site (see Materials and methods for details on the model). The model therefore has to fit two rate constants, the exchange rate between bud and mother of free Myo4p and the dissociation rate of bound Myo4p in wt buds. Both *she2Δ* and wt FLIPs could be fit by a similar rate constant for diffusive exchange of free Myo4p, $k_{diff} = 0.082 \pm 0.009\ s^{-1}$ (*she2Δ*) and $k_{diff} = 0.071 \pm 0.033\ s^{-1}$ (wt). For the dissociation rate of bound Myo4p in wt cells, the model could only extract a lower limit, because the depletion kinetics were such that any $k_{off} > 0.1\ s^{-1}$ produced a good fit (Fig. 7 B). Computer simulations with different k_{off} values ranging from 10 to $0.005\ s^{-1}$ showed that a dissociation constant $<0.01\ s^{-1}$ would severely distort the depletion kinetics and result in curves well outside the standard deviation of the

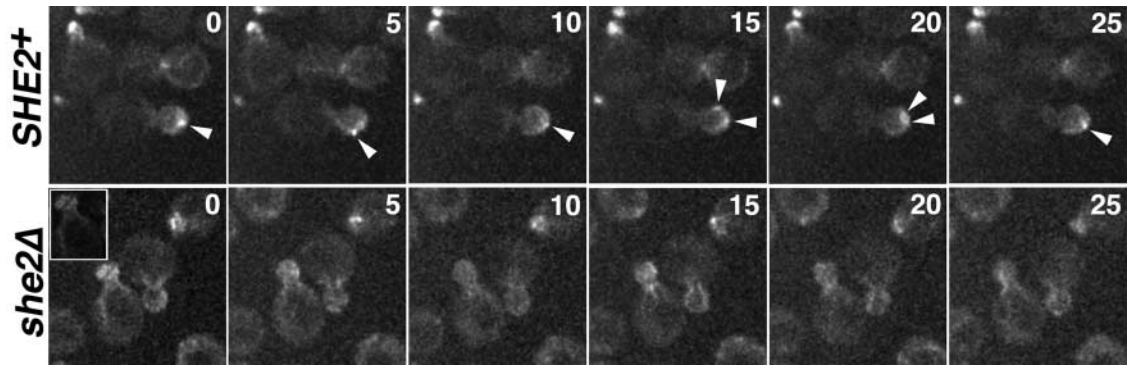

Figure 6. **Bud-restricted movement of Myo4–GFP particles.** Stills from movies (Videos 1 and 2, available at http://www.jcb.org/cgi/content/full/jcb.200207101/DC1) showing Myo4–GFP in wt cells (RJY1310) or *she2Δ* cells (RJY1405) followed by time-lapse confocal microscopy. Projections of stacks acquired every 5 s (numbers in upper right corners correspond to time) are shown. Arrowheads point to larger Myo4–GFP-containing particles that move along the bud cortex in wt cells. Note that the bottom images were acquired with increased gain settings. Insert in lower left panel (*she2Δ*, 0 s) shows Myo4–GFP signal intensity in *she2Δ* mutant cells with identical gain settings as those used for wt cell imaging.

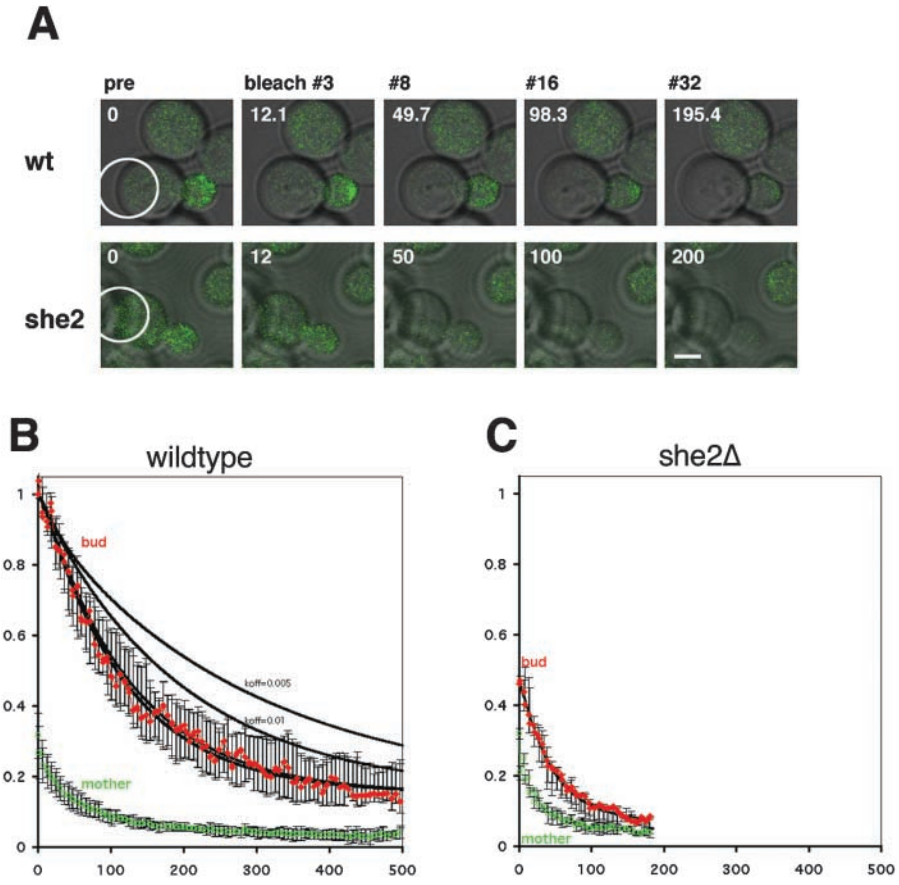

Figure 7. **FLIP of Myo4–GFP in wt and *she2Δ* cells.** (A) Representative confocal images of a FLIP experiment. The bleached region in the mother cell is indicated in the first frame before the first bleach. The number of bleaches and time in seconds are indicated. Contrast for the dimmer *she2Δ* cells was enhanced for visualization. Bar, 2 μm. (B) Depletion of mean Myo4–GFP fluorescence of bud (red) and mother (green) in wt cells for experiments such as shown in A. Error bars indicate the standard deviation of $n = 8$ experiments. Black lines show the curve fits of the computer simulation to a single data set; in this case, $k_{diff} = 0.09$ and k_{off} varied from 10 to 0.005 s^{-1}. Note the excellent fits to the data for high values of k_{off} and the distortion of the fit beyond the standard deviation by $k_{off} > 0.01$. (C) Like B, for *she2Δ* cells. Only the fit for $k_{diff} = 0.088$ is given, because in *she2Δ* cells, no strong enrichment of Myo4–GFP in the bud is observed that would suggest to fit k_{off}. For comparison, the initial fluorescence intensity in the mother is normalized to the same value as for the mother in wt cells shown in B.

FLIP measurements (Fig. 7 B). Our results are thus consistent with the conclusion that the exchange of free Myo4–GFP between bud and mother is limited by diffusion in both *she2Δ* and wt cells. A binding interaction that could be responsible for the retention and steady-state accumulation of Myo4–GFP in the bud of wt cells would have a $k_{off} > 0.01\ s^{-1}$, i.e., a mean residency time at the binding site of <100 s. These results suggest that the retaining interaction of Myo4–GFP in the bud of wt cells is short lived and dynamically exchanges with the soluble pool in both bud and mother cell.

Discussion

In vivo approaches that followed the trafficking of myosin-V cargo suggest that yeast class V myosins move along tracks from the mother cell to the bud (Bertrand et al., 1998; Schott et al., 2002). However, under steady-state conditions, both Myo2p and Myo4p are mainly found at the bud tip with little staining in the cytoplasm (Lillie and Brown, 1994; Schott et al., 1999; Catlett et al., 2000; Karpova et al., 2000). Only a small fraction of yeast myosin-V has been detected on filamentous structures that resemble actin cables (Münchow et al., 1999), suggesting that there might be a yet unknown mechanism that leads to the enrichment of myosin motor proteins at the bud tip.

RNP- versus She2p-dependent distribution of Myo4p

We have found that the loss of She3p and She2p results in the loss of Myo4p accumulation at the bud cortex. Although we cannot exclude the possibility that lack of She2p or She3p results in misfolded Myo4–GFP that is unable to localize, it seems unlikely because Myo4p levels do not change upon deletion of *SHE2* or *SHE3*. Because misfolded proteins are quickly removed from the cytoplasm (Bukau et al., 2000), reduced Myo4p levels would be expected if misfolding is caused by the absence of She2p or She3p. Instead, four lines of evidence indicate that Myo4p accumulation requires not only the RNA-binding protein She2p but a complex of the RNA-binding protein and its cognate mRNAs. First, we have previously shown that She2p alone shows only weak association with She3p and Myo4p in vivo and that efficient binding to the Myo4p–She3p complex requires the expression of localized mRNAs (Böhl et al., 2000). Second, a truncated She2p unable to bind RNA is incapable of promoting Myo4–GFP localization. This mutant is also unable to associate with the Myo4p–She3p complex (unpublished data), possibly because it requires mRNA binding to do so. Third, blocking nuclear mRNA export in an *mex67-5^{ts}* mutant resulted in a partial nuclear accumulation of She2p. Previous studies showed that under the conditions we used to inactivate mRNA export, poly(A)$^+$ RNA is mainly nuclear (Segref et al., 1997), suggesting that the remaining cytoplasmic She2p is not bound to mRNA. The cytoplasmic fraction cannot support Myo4–GFP localization to the bud. Finally, She2p is dispensable if mRNA is directly targeted to the Myo4p–She3p complex via MS2 RNA–MS2 protein interaction. In agreement with previ-

ous findings (Long et al., 2000), these data in summary suggest that She2p might simply function as a linker between localized mRNAs and the motor protein complex and that association with mRNA is key to Myo4p localization. It is nevertheless striking that we did not see a significant decrease of Myo4–GFP signal in cells lacking the two cargo mRNAs *ASH1* and *IST2*. The main reason for this might be the high degree of fluorescence intensity variation in both the wild type and double mutant, which makes it impossible to identify significant differences. Coimmunoprecipitation experiments of Myo4p and She2p with associated mRNAs suggested that 11 different mRNAs might be bound by the Myo4–She complex (Takizawa et al., 2000). Deletion of only two of those could therefore be expected to result in a milder effect than disruption of the RNA-binding protein She2p.

Shuttling of the RNA-binding protein She2p

Several findings suggest that the RNA-binding protein She2p is shuttling between the nucleus and cytoplasm. A number of other proteins involved in mRNA localization show similar shuttling behavior (Cote et al., 1999; Munro et al., 1999; Norvell et al., 1999; Shyu and Wilkinson, 2000; Hachet and Ephrussi, 2001; Gu et al., 2002). However, in contrast to She2p, the equilibrium of most of these proteins is shifted toward the nuclear compartment with only little protein in the cytoplasm (Cote et al., 1999; Munro et al., 1999; Norvell et al., 1999; Hachet and Ephrussi, 2001; Gu et al., 2002).

Although mainly cytoplasmic, She2p is never excluded from nuclei, even in wt cells (Böhl et al., 2000; Fig. 4), indicating that a minor fraction of the She2p pool is nuclear. The 28-kD She2 protein is theoretically small enough to enter the nucleus by passive diffusion, but an association of She2p with yeast importin α (Srp1p) has recently been detected (Ito et al., 2001), suggesting that She2p might be actively imported into the nucleus. However, nuclear localization signals within She2p have not yet been mapped.

Nuclear accumulation of She2p was observed under two circumstances, deletion of a region of the protein essential for RNA binding and inhibition of nuclear export in an *mex67-5* mutant. Neither Mex67p nor its metazoan homologue TAP have so far been implicated in nuclear protein export but are essential for mRNA export (Lei and Silver, 2002), making it unlikely that Mex67p is directly exporting She2p. Rather, the two results suggest that export of She2p from the nucleus requires its association with RNA. We would propose from our data that She2p binds to its cognate mRNAs already in the nucleus and is subsequently "piggyback" exported via mRNA-mediated export pathways where it assembles with the She3p–Myo4p complex.

Retention of Myo4p in the bud depends on association with an She2p RNP

How could the association of a myosin motor with its RNP cargo control the distribution of the motor? We have shown that the absence of the RNA-binding protein She2p results in the loss of Myo4–GFP signal at the tip of larger buds. Time-lapse life imaging of Myo4–GFP in *she2Δ* cells suggested that Myo4p is able to enter the bud even in the absence of She2p (at least during early cell cycle stages) but that particles containing Myo4–GFP rapidly disintegrate. FLIP experiments show that Myo4–GFP in *she2Δ* mutant cells constantly and rapidly cycles between bud and mother cell. It is conceivable that the association with an RNP leads to retention of the myosin at the bud cortex and concentrates it there. This retention is of a transient nature, however, as FLIP experiments show that even in wt cells, Myo4–GFP can still cycle between bud and mother efficiently and that the retaining interaction has a mean lifetime of <2 min. Because the yeast actin cytoskeleton is polarized during most of the cell cycle such that myosins can only actively move along filaments from the mother cell into the bud, we would implicate diffusion as the driving force for the observed retrograde movement of Myo4–GFP.

The observed difference of Myo4p accumulation in the presence or absence of the RNP cargo could be explained by a more efficient transport of Myo4p to the bud in the presence of its RNP cargo, by a transient retention of the motor in the bud by the cargo, or by a combination of both mechanisms. Because Myo4p appears to be a nonprocessive motor, RNP cargo might simply cross-link several Myo4p molecules, allowing efficient trafficking of the myosin. This model would be attractive because *ASH1* mRNA contains several localization elements that can all be recognized by She2p (Chartrand et al., 2001). However, in the absence of Myo4p's cognate cargo, a hybrid RNA of lacZ–MS2 RNA bound to the Myo4–She3p complex via a single RNA binding site also leads to Myo4–GFP accumulation at the bud tip, which argues against a cross-linking function of the cargo. In addition, a second cognate cargo mRNA of Myo4p, *IST2*, contains only one localization element that is recognized by She2p (unpublished data).

Although we cannot formerly exclude that cargo influences forward transport of the myosin, our data suggest that cargo rather influences retention of the motor at the bud cortex. If the RNP cargo is responsible for transient retention of Myo4p, what could be the molecular basis of this retention? Once transported, *ASH1* mRNA is anchored at the bud tip (Chartrand et al., 2001). Besides the RNA-binding protein Khd1p (Irie et al., 2002), translation has been implicated in anchoring because *ASH1* mRNA is diffusely distributed inside the bud if its AUG codon is mutated or premature nonsense codons are inserted (Gonzalez et al., 1999; Irie et al., 2002). Although the molecular mechanism behind this phenomenon is unclear, it is conceivable that association with the translational apparatus might not only retain localized mRNAs but, transiently, also the transport machinery associated with it, including the motor protein. Consistent with this idea, we have observed that brief treatment with the translational inhibitor cycloheximide results in loss of both cortically localized *ASH1* mRNA and HA-tagged Myo4p and redistribution of both factors to small particles in the bud cytoplasm (see Fig. S3, available online at http://www.jcb.org). Because cycloheximide inhibits translation elongation but stabilizes polyribosomes, it might be that an active translation process, and not only association of localized mRNAs with polyribosomes, is required for Myo4p's accumulation at the bud cortex.

Myo4p is believed to transport its cargo into the bud along actin cables, and it has been shown that an *MS2–ASH1* RNP particle moves in an Myo4p-dependent manner from the mother cell into the bud (Bertrand et al., 1998; Beach et al., 1999). Why didn't we detect the directed movement of Myo4–GFP particles from the mother to the bud? Although we cannot rule out other explanations, one possible reason might be that in previous work, overexpressed reporter mRNAs were used to facilitate real-time observation of the rapid movement (Bertrand et al., 1998). Such overexpression might have led to the incorporation of most *MS2–ASH1* RNA and Myo4p into a single bright particle. In a wt situation that we have studied, *ASH1* or *IST2* mRNA have never been detected in single particles by in-situ hybridization but appear as multiple smaller particles (Long et al., 1997; Takizawa et al., 1997, 2000). It is conceivable that under such conditions Myo4–GFP movement toward the bud is simply not detectable because the fluorescence signal of single moving particles might be too weak. Only once Myo4–GFP-containing complexes have assembled into larger particles at the cortex would they become detectable. Consistent with this idea, a GFP fusion of the second class V myosin Myo2p is not detectable during transit along actin filaments and can only be seen in large clusters at the bud cortex (Karpova et al., 2000). In addition, Sec4–GFP-containing vesicles that travel in an Myo2-dependent manner to the bud are hardly detectable during transit and 30–200 times weaker in fluorescence than the Sec4–GFP signal found at the bud tip (Schott et al., 2002).

In summary, we propose a model in which localization of the yeast class V myosin Myo4p at the bud tip is explained by transient accumulation, and this accumulation depends on its association with its RNP cargo. Such cargo effects do not come without precedent. There are recent examples of kinesin motor localization controlled by nonmotor subunits or cargo proteins. Differential localization of the yeast kinesin-related protein Kar3p depends on its association with nonmotor subunits Cik1p or Vik1p (Manning et al., 1999). Targeting of mouse KIF5 to the dendritic compartment in neurons depends on association with the cargo component GRIP1 (Setou et al., 2002). Is the localization of class V myosins, other than Myo4p, also dependent on their association with cargo? Yeast Myo2p mutants that cannot interact with vesicular cargo still accumulate at the bud tip (Schott et al., 1999). However, mutations in *MYO2* affecting polarized vesicle delivery do not interfere with a second function, vacuole inheritance (Catlett et al., 2000), suggesting that, similar to different RNA cargo in the case of Myo4p, different cargo might be able to interact with Myo2p and help to concentrate it at the bud tip. The situation for vertebrate class V myosins is even less clear, but the recent identification of myosin-V receptors on cargo vesicles (Karcher et al., 2002) provides the means to tackle the question of cargo-dependent myosin localization in higher eukaryotes as well.

Materials and methods

General

General methods to culture and manipulate yeast strains were used as previously described (Gietz and Schiestl, 1991; Adams et al., 1997). The preparation of cell extracts for Western blotting was performed as previously published (Böhl et al., 2000).

Plasmids

Plasmid RJP543 (pUC19–2xGFP::klTRP1) that served as the template for PCR-based double EGFP tagging of *MYO4* was constructed as follows. A 1.4-kbp DNA fragment containing a tandem cassette of two GFP (S65T, V163A) open reading frames was amplified from template pSF24-2xGFP (a gift from S. Frey, Zentrum für Molekulare Biologie der Universität Heidelberg) using primers RJO837 and RJO838, each providing a NheI site at its 5′ end. After digesting, the fragment was cloned into the NheI site of pWZ86 (a gift from W. Zachariae, Max Planck Institute of Molecular Cell Biology and Genetics, Dresden, Germany), generating RJP543. The tandem GFP cassette and a 3′ UTR lie upstream of the *TRP1* gene from *Kluveromyces lactis* that becomes part of the tagging module and serves as a selectable marker after transformation.

Plasmid RJP629, expressing an NH_2-terminally truncated She2p, was created by amplifying the *SHE2* promotor using primers RJO447 and RJO992 and its coding region plus 3′ UTR using the primer pair RJO446 and RJO992. RJO991 and RJO992 introduce NcoI sites that allow ligation of the corresponding fragments and generate a new AUG 213 bp downstream of the original AUG. The ligated product was digested with HindIII and cloned into YCplac22 (Gietz and Sugino, 1988). The mutant allele was called *SHE2ΔN70*. An Nsi1–Sph1 fragment was released and cloned into plasmid RJP578 (Ycplac22-*SHE2–myc3*) to construct a myc-tagged version of *SHE2ΔN70*. The gene was released from the resulting plasmid and inserted as a HindIII fragment into YEplac181 (Gietz and Sugino, 1988), thus generating plasmid RJP629. The generation of the remaining plasmids (expressing lacZ–MS2 hybrid RNAs or 2μ-*ASH1*) is explained in the supplementary Materials and methods, available at http://www.jcb.org/cgi/content/full/jcb.200207101/DC1.

Yeast strains

A complete list of strains used during this study is shown in Table I. Yeast strain backgrounds were either W303 (*Mat**a** ade2-1 trp1-1 can1-100 leu2-3,112 his3-11,15 ura3 GAL psi+*) or, in the cases of *MEX67* or *mex67-5*^{ts} strains, RS453 (*Mat**a** ade2-1 his3 leu2 trp1 ura3 his3*).

Yeast strains RJY1303, RJY1304, RJY1310, RJY1405, RJY1343, RJY1526, RJY1528, and RJY1624 that express a fusion of Myo4p with two GFP proteins were generated by PCR-based epitope tagging of *MYO4* at the genomic locus, using plasmid RJP543 as a template and oligos RJO61 and RJO62 to generate the PCR product used for transformation.

Epitope-tagged alleles of *MYO4* and *SHE2* in an *mex67-5*^{ts} mutant strain were generated by a PCR-based method (Knop et al., 1999). Gene deletions of *SHE2*, *ASH1*, or *IST2* using the *HIS3MX6* cassette (Wach et al., 1997) or a *Kluveromyces lactis TRP1* marker in strains RJY1526, RJY1528, RJY1624, RJY1640, and RJY1641 were created by a similar PCR-based gene disruption. Disruption of *SHE2* or *SHE3* with a *URA3* marker has been described elsewhere (Jansen et al., 1996). Strains RJY1528 and RJY1600 were derived by transformation of pSHE2ΔN70-myc (RJP629) into cells bearing *she2* deletions. Strains RJY1526 and RJY1599 were generated similarly using pSHE2-myc (RJP627). Strain RJY1613 (*SHE2*–myc9 *MYO4*–HA6 *mex67-5 GAL1–ASH1*) was created by crossing strains RJY1164 and RJY1578 and selection for the appropriate allele combination, followed by transformation with plasmid RJP309 (p*GAL1-ASH1*; Böhl et al., 2000). A detailed description of each strain generation will be available upon request.

Temperature shift experiments

MEX67 or *mex67-5* cells expressing Myo4–GFP were grown to exponential growth phase at 26°C in SC-trp 2% glucose. Cells were harvested by low speed centrifugation and resuspended to cell densities of $<10^7$ cells/ml in 37°C prewarmed medium. After a 30-min incubation, cells were collected, resuspended in medium at 26°C, and further incubated for 20 min. Aliquots were taken at different time points and directly inspected by fluorescence microscopy. Myo2p was detected using a polyclonal anti-Myo2p antibody (a gift from S. Reck-Peterson, Yale University, New Haven, CT) and actin was detected using the monoclonal rat antibody C4 (Roche Diagnostics).

To simultaneously detect Myo4p–HA6 and She2p–myc9 in *mex67-5* cells, strain RJY1613 was grown overnight in SC-trp 2% raffinose and diluted into YEP + 2% galactose in order to induce *ASH1* mRNA expression from plasmid p*GAL1-ASH1* (RJP309). After a 3-h induction at 26°C, cells were transferred into 37°C prewarmed medium. After a 30-min incubation, cells were fixed and prepared for immunofluorescence microscopy as described below.

Table I. **Yeast strains**

Strain	Background[a]	Relevant genotype	Source
RJY375	W303	*MATa pep4::URA3 CSE1-myc9::HIS3* YEplac181-*ASH1*	Münchow et al. (1999)
RJY1004	W303	*MATα HO-ADE2 HO-CAN1 SHE3-myc6 ash1Δ::TRP1 ist2Δ::HIS3MX6*	This study
RJY1164	RS453	*MATa mex67::HIS3 SHE2-myc9::klTRP1* pUN100-*mex67-5*	This study
RJY1303	RS453	*MATa mex67:HIS3 MYO4-2xGFP::klTRP1* pUN100-*mex67-5*	This study
RJY1304	W303	*MATa she3Δ::URA3 MYO4-2xGFP::klTRP1*	This study
RJY1310	W303	*MATa MYO4-2xGFP::klTRP1*	This study
RJY1405	W303	*MATa she2Δ::URA3 MYO4-2xGFP::klTRP1*	This study
RJY1343	RS453	*MATa mex67:HIS3 MYO4-2xGFP::klTRP1* pUN100-*MEX67*	This study
RJY1526	W303	*MATa she2Δ::HIS3MX6 MYO4-2xGFP::klTRP1* YEplac181-*SHE2-myc3*	This study
RJY1528	W303	*MATa she2Δ::HIS3MX6 MYO4-2xGFP::klTRP1* Yeplac181-*SHE2ΔN70-myc3*	This study
RJY1578	RS453	*MATa SHE2-myc3::HIS3MX6 MYO4-HA6::klTRP1*	This study
RJY1581	W303	*MATa MYO4-HA6* pRS316-*pADH1-ASH1*	This study
RJY1599	W303	*MATα HO-ADE2 HO-CAN1 she2Δ::URA3* YEplac181-*SHE2-myc3* YEplac112-*ASH1*	This study
RJY1600	W303	*MATα HO-ADE2 HO-CAN1 she2Δ::URA3* YEplac181-*SHE2ΔN70-myc3* YEplac112-*ASH1*	This study
RJY1613	RS453	*MATα mex67::HIS3 SHE2-myc9::klTRP1 MYO4-HA6::klTRP1* pUN100-*mex67-5* pRS426-*GAL1-ASH1*	This study
RJY1624	W303	*MATa MYO4-2xGFP::klTRP1 ash1::TRP1 ist2::HIS3MX6*	This study
RJY1640	W303	*MATa she2Δ::HIS3MX6 MYO4-2xGFP::klTRP1* YEplac181-*SHE3-MS2* YEplac195-*GAL1-lacZ-ADHII*	This study
RJY1641	W303	*MATa she2Δ::HIS3MX6 MYO4-2xGFP::klTRP1* Yeplac181-*SHE3-MS2* YEplac195-*GAL1-lacZ-MS2(6)-ADHII*	This study
RJY1813	W303	*MATa she2Δ::HIS3MX6 MYO4-2xGFP::klTRP1* Yeplac181-*SHE3-MS2* YEplac195-*GAL1-lacZ-MS2(1)-ADHII*	This study

[a]Strains of W303 background are derivatives of W303a (also named K699) with the full genotype *Mata, ade2-1, trp1-1, can1-100, leu2-3,112, his3-11,15, ura3, GAL, psi*$^+$. The full genotype of RS453 strain background is *Mata, ade2, his3, leu2, trp1, ura3, his3*.

Fluorescence microscopy

Indirect double immunofluorescence against myc- or HA-tagged proteins and in-situ hybridization against *ASH1* mRNA were essentially done as previously described (Böhl et al., 2000). In brief, exponentially growing cells of strain RJY1613 were fixed after induction of *ASH1* expression in YEP + 2% galactose medium before and after temperature shift by adding formaldehyde (4% final concentration) to the culture medium. Cells were fixed for 60 min at the corresponding temperature, pelleted, washed, and spheroplasted using oxalyticase (Enzogenetics). Spheroplasts were attached to poly-L-lysine–coated multiwell slides and sequentially incubated with mouse anti-myc antibody (9E10; Roche), rabbit anti–mouse IgG coupled to Alexa®488 (Molecular Probes), rat anti-HA antibody (3F10; Roche), and goat anti–rat IgG coupled to Alexa®594 (Molecular Probes). Nuclei were stained with DAPI, and cells were mounted in 80% glycerol.

For widefield fluorescence microscopy of cells expressing Myo4–GFP, cultures were grown in SC-trp to cell densities below 10^7 cells/ml. 3 μl of each culture were dropped onto a microscope slide coated with a pad of SC-trp 2% agarose that had been trimmed to a 15 × 15-mm square and a coverslip was applied. Images were acquired directly after adding cells to agarose pads (usually in the first 2–4 min), but cells were found to be viable and able to divide for at least 6 h under these conditions. For observation of GFP signals in temperature shift experiments, agarose pads were equilibrated to 37°C or 26°C before cells were applied. Cells were inspected with an Olympus BX60 fluorescence microscope (Olympus) and a 100× NA 1.3 DIC oil objective. Images were acquired using an ORCA ER CCD camera (Hamamatsu Photonics) controlled by Openlab 3.01 software (Improvision). For the quantification of Myo4–GFP in wild type, *she2Δ*, *she3Δ*, and *ash1Δ/ist2Δ* cells, images of 150 cells with medium-sized buds (~2-μm diameter) were acquired. Fluorescence in the bud and a corresponding area in the mother cell were determined using the measurement function of the Openlab software package. The area in the mother cell was selected not to contain a vacuole or nucleus. After background subtraction, the average fluorescence and standard deviation were determined with Microsoft Excel.

Live cell imaging

Time-lapse imaging of *MYO4–GFP* strains RJY1310 (wt) or RJY1405 (*she2Δ*) at 30°C was performed using a PerkinElmer Ultraview confocal microscope equipped with a Nikon 100× NA 1.3 oil objective (PerkinElmer). Cells were attached to coverslip chambers (MatTek) coated with 5 mg/ml ConA and directly observed in SC-trp medium. Due to the weak signal of Myo4–GFP, only five focal planes (0.5-μm distance in Z) per stack were acquired with a 450-ms exposure time at 2 × 2 binning, resulting in a total acquisition time of 2.5 s per stack. A total of 50 stacks were acquired per experiment (125 s total). Focal planes of each stack were projected by maximum intensity projection using the ImageJ software package (NIH). Before exporting as Quicktime movies, the resulting images were filtered to remove noise. Single frames from representative movies were exported into Adobe Photoshop 6® and assembled.

FLIP and kinetic modeling

FLIP was performed on an LSM 510 confocal microscope essentially as previously described (Ellenberg et al., 1997; Daigle et al., 2001). The LSM 510 was fitted with selected PMTs (Carl Zeiss MicroImaging, Inc) and custom dichroics and emission filters (Chroma Technology Corp.) for fluorescent protein imaging using a PlanApochromat 63× NA 1.4 oil DIC objective (Carl Zeiss MicroImaging, Inc) and an optical section of 2.5 μm (FWHM). Circular bleach regions were defined to cover ~50% of the mother cell, taking care not to directly bleach the bud itself (Fig. 7). Low intensity scanning to monitor intensity changes after bleaching did not significantly reduce fluorescence over the time of the experiment, as verified in control cells in the same field (not depicted). Bleaching was performed at an intensity 200 times higher than scanning.

To extract kinetic parameters from FLIP experiments, we used a simple numerical computer simulation for flux between two compartments, mother and bud (see schematic below). The exchange between mother and bud is governed by a single bidirectional rate constant k_{diff}, assuming diffusion. The situation in *she2Δ* cells is taken as steady state in the absence of any binding interactions achieved by diffusive equilibration between bud and mother. For wt cells, the additional Myo4–GFP enriched in the bud (a fraction of ~55% of the bud material) is assumed to be bound to a hypothetical Myo4p receptor and has to dissociate with a dissociation constant k_{off} to enter the free pool in the bud (a fraction of 45% of the bud material), which in turn can exchange with the mother cell that is depleted at a constant rate k_{bleach} by the FLIP experiment. Because the concentration of the receptor is unknown, the model uses only the product of the association constant and receptor concentration, which is given by k_{on} *

[Myo4p–R] = k_{off} * (bound/free). The simulation used coupled differential equations to fit the experimental data and was programmed in Berkeley Madonna (George Oster, University of California at Berkeley, Berkeley, CA; www.berkeleymadonna.com).

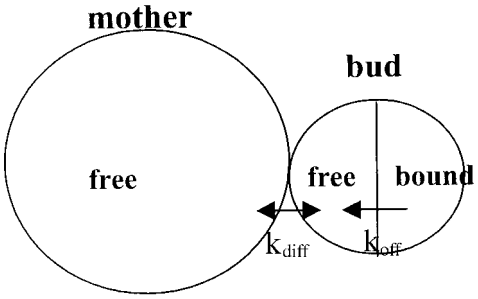

mRNA coimmunoprecipitation

Protein–mRNA coimmunoprecipitation was essentially done as previously described (Münchow et al., 1999; Böhl et al., 2000; Long et al., 2000). In brief, cells of strains RJY375, RJY1599, or RJY1600 expressing Cse1–myc or myc-tagged She2p (either wt or She2pΔN70) were grown to exponential growth phase, and 8×10^9 cells were harvested and disrupted using glass beads. After removing an aliquot that served as the input control, the resulting extract was incubated sequentially with monoclonal anti-myc antibody and protein G–Sepharose 6FF (Amersham Biosciences). Immunocomplexes were collected by a brief spin at 500 *g* and washed, and RNAs were eluted with 1% SDS and extracted with phenol–chloroform. 1/18 of total RNA (input) and 1/2 of coprecipitated RNAs were applied to a nylon membrane with a Minifold dot blotter (Schleicher & Schuell). The membrane was stained with methylene blue and hybridized with a probe against *ASH1*. 1/18 of total RNA from a strain that carries deletions of *ASH1* and *IST2* (RJY1004) served as a control to compensate for unspecific hybridization of the probe used for hybridization.

Online supplemental material

A list of plasmids as well as oligonucleotides used in this study (Table S1) is available online at http://www.jcb.org/cgi/content/full/jcb.200207101/DC1. Three supplementary figures (Figs. S1–S3) and Quicktime movies showing the dynamic distribution of Myo4–GFP in wt (Video 1) and *she2Δ* cells (Video 2) are also available.

We thank P. Chartrand (Albert Einstein College of Medicine, New York, NY), S. Frey, E. Hurt (Biochemie-Zentrum Heidelberg, Germany), M. Knop (European Molecular Biology Laboratory, Heidelberg, Germany), R. Long (Medical College of Wisconsin, Milwaukee, WI), and W. Zachariae for plasmids and strains, E. Busch and T. Zimmermann for help with real-time fluorescence microscopy, and S. Reck-Peterson for anti-Myo2p antibodies. We also thank D. Brunner and M. Seedorf for comments on the manuscript.

R.-P. Jansen is a recipient of grants from the Deutsche Forschungsgemeinschaft (JA696/2 and JA696/4-1). J. Ellenberg acknowledges support from the Human Frontier Science Program Organization (RGP0031/2001-M). J. Beaudouin was supported by a predoctoral fellowship of European Molecular Biology Laboratory's international Ph.D. program.

Submitted: 17 July 2002
Revised: 7 November 2002
Accepted: 7 November 2002

References

Adams, A., D.E. Gottschling, C.A. Kaiser, and T. Stearns. 1997. Methods in Yeast Genetics. Cold Spring Harbor Laboratory Press, Cold Spring Harbor, NY. 1–177.

Ayscough, K.R., J. Stryker, N. Pokala, M. Sanders, P. Crews, and D.G. Drubin. 1997. High rates of actin filament turnover in budding yeast and roles for actin in establishment and maintenance of cell polarity revealed using the actin inhibitor latrunculin-A. *J. Cell Biol.* 137:399–416.

Bähler, M., and A. Rhoads. 2002. Calmodulin signaling via the IQ motif. *FEBS Lett.* 513:107–113.

Beach, D.L., E.D. Salmon, and K. Bloom. 1999. Localization and anchoring of mRNA in budding yeast. *Curr. Biol.* 9:569–578.

Bertrand, E., P. Chartrand, M. Schaefer, S.M. Shenoy, R.H. Singer, and R.M. Long. 1998. Localization of ASH1 mRNA particles in living yeast. *Mol. Cell.* 2:437–445.

Bobola, N., R.-P. Jansen, T.H. Shin, and K. Nasmyth. 1996. Asymmetric accumulation of Ash1p in postanaphase nuclei depends on a myosin and restricts yeast mating-type switching to mother cells. *Cell.* 84:699–709.

Böhl, F., C. Kruse, A. Frank, D. Ferring, and R.-P. Jansen. 2000. She2p, a novel RNA-binding protein tethers *ASH1* mRNA to the Myo4p myosin motor via She3p. *EMBO J.* 19:5514–5524.

Boyne, J.R., H.M. Yosuf, P. Bieganowski, C. Brenner, and C. Price. 2000. Yeast myosin light chain, Mlc1p, interacts with both IQGAP and class II myosin to effect cytokinesis. *J. Cell Sci.* 113:4533–4543.

Bukau, B., E. Deuerling, C. Pfund, and E.A. Craig. 2000. Getting newly synthesized proteins into shape. *Cell.* 101:119–122.

Catlett, N.L., and L.S. Weisman. 1998. The terminal tail region of a yeast myosin-V mediates its attachment to vacuole membranes and sites of polarized growth. *Proc. Natl. Acad. Sci. USA.* 95:14799–14804.

Catlett, N.L., J.E. Duex, F. Tang, and L.S. Weisman. 2000. Two distinct regions in a yeast myosin-V tail domain are required for the movement of different cargoes. *J. Cell Biol.* 150:513–525.

Chartrand, P., R.H. Singer, and R.M. Long. 2001. RNP localization and transport in yeast. *Annu. Rev. Cell Dev. Biol.* 17:297–310.

Cote, C.A., D. Gautreau, J.M. Denegre, T.L. Kress, N.A. Terry, and K.L. Mowry. 1999. A *Xenopus* protein related to hnRNPI has a role in cytoplasmic RNA localization. *Mol. Cell.* 4:431–437.

Daigle, N., J. Beaudouin, G. Hartnell, E. Imreh, J. Hallberg, J. Lippincott-Schwartz, and J. Ellenberg. 2001. Nuclear pore complexes form immobile networks and have a very low turnover in mammalian cells. *J. Cell Biol.* 154: 71–84.

Ellenberg, J., E.D. Siggia, J.E. Moreira, C.L. Smith, J.F. Presley, H.J. Worman, and J. Lippincott-Schwartz. 1997. Nuclear membrane dynamics and reassembly in living cells: targetting of an inner nuclear membrane protein in interphase and mitosis. *J. Cell Biol.* 138:1193–1206.

Gietz, R.D., and R.H. Schiestl. 1991. Application of high efficiency lithium acetate transformation of intact yeast cells using single-stranded nucleic acids as carrier. *Yeast.* 7:253–263.

Gietz, R.D., and A. Sugino. 1988. New yeast-*Escherichia coli* shuttle vectors constructed with in vitro mutagenized yeast genes lacking six-base pair restriction sites. *Gene.* 74:527–534.

Gonzalez, I., S.B.C. Buonomo, K. Nasmyth, and U. von Ahsen. 1999. *ASH1* mRNA localization in yeast involves multiple secondary structural elements and Ash 1 protein translation. *Curr. Biol.* 9:337–340.

Govindan, B., R. Bowzer, and P. Novick. 1995. The role of Myo2, a yeast class V myosin, in vesicular transport. *J. Cell Biol.* 128:1055–1068.

Gu, W., F. Pan, H. Zhang, G. Bassell, and R.H. Singer. 2002. A predominantly nuclear protein affecting cytoplasmic localization of β-actin mRNA in fibroblasts and neurons. *J. Cell Biol.* 156:41–51.

Hachet, O., and A. Ephrussi. 2001. *Drosophila* Y14 shuttles to the posterior of the oocyte and is required for *oskar* mRNA transport. *Curr. Biol.* 11:1666–1674.

Hirokawa, N. 1998. Kinesin and dynein superfamily proteins and the mechanism of organelle transport. *Science.* 279:519–526.

Hurt, E., K. Strasser, A. Segref, S. Bailer, N. Schlaich, C. Presutti, D. Tollervey, and R. Jansen. 2000. Mex67p mediates nuclear export of a variety of RNA polymerase II transcripts. *J. Biol. Chem.* 275:8361–8368.

Irie, K., T. Tadauchi, P.A. Takizawa, R.D. Vale, K. Matsumoto, and I. Herskowitz. 2002. The Khd1 protein, which has three KH RNA-binding motifs, is required for proper localiaztion of *ASH1* mRNA in yeast. *EMBO J.* 21: 1158–1167.

Ito, T., T. Chiba, R. Ozawa, M. Yoshida, M. Hattori, and Y. Sakaki. 2001. A comprehensive two-hybrid analysis to explore the yeast protein interactome. *Proc. Natl. Acad. Sci. USA.* 98:4569–4574.

Jansen, R.-P., C. Dowzer, C. Michaelis, M. Galova, and K. Nasmyth. 1996. Mother cell-specific HO expression in budding yeast depends on the unconventional myosin Myo4p and other cytoplasmic proteins. *Cell.* 84:687–697.

Johnston, G.C., J.A. Prendergast, and R.A. Singer. 1991. The *Saccharomyces cerevisiae* MYO2 gene encodes an essential myosin for vectorial transport of vesicles. *J. Cell Biol.* 113:539–551.

Karcher, R.L., S.W. Deacon, and V.I. Gelfand. 2002. Motor-cargo interactions:

the key to transport specificity. *Trends Cell Biol.* 12:21–27.

Karpova, T.S., S.L. Reck-Peterson, N.B. Elkind, M.S. Mooseker, P.J. Novick, and J.A. Cooper. 2000. Role of actin and Myo2p in polarized secretion and growth of *Saccharomyces cerevisiae*. *Mol. Biol. Cell.* 11:1727–1737.

Knop, M., K. Siegers, G. Pereira, W. Zachariae, B. Winsor, K. Nasmyth, and E. Schiebel. 1999. Epitope tagging of yeast genes using a PCR-based strategy: more tags and improved practical routines. *Yeast.* 15:963–972.

Lei, E.P., and P.A. Silver. 2002. Protein and RNA export from the nucleus. *Dev. Cell.* 2:261–272.

Lillie, S.H., and S.S. Brown. 1994. Immunofluorescence localization of the unconventional myosin, Myo2p, and the putative kinesin-related protein, Smy1p, to the same regions of polarized growth in *Saccharomyces cerevisiae*. *J. Cell Biol.* 125:825–842.

Lippincott-Schwartz, J., E. Snapp, and A. Kenworthy. 2001. Studying protein dynamics in living cells. *Nat. Rev. Mol. Cell Biol.* 2:444–456.

Long, R.M., R.H. Singer, X. Meng, I. Gonzalez, K. Nasmyth, and R.-P. Jansen. 1997. Mating type switching in yeast controlled by asymmetric localization of *ASH1* mRNA. *Science.* 277:383–387.

Long, R.M., W. Gu, E. Lorimer, R.H. Singer, and P. Chartrand. 2000. She2p is a novel RNA-binding protein that recruits the Myo4p/She3p complex to *ASH1* mRNA. *EMBO J.* 19:6592–6601.

Manning, B.D., J.G. Barret, J.A. Wallace, H. Granok, and M. Snyder. 1999. Differential regulation of the Kar3p kinesin-related protein by two associated proteins, Cik1p and Vik1p. *J. Cell Biol.* 144:1219–1233.

Mehta, A.D., R.S. Rock, M. Rief, J.A. Spudich, M.S. Mooseker, and R.E. Cheney. 1999. Myosin-V is a processive actin-based motor. *Nature.* 400:590–593.

Mermall, V., P.L. Post, and M.S. Mooseker. 1998. Unconventional myosins in cell movement, membrane traffic, and signal transduction. *Science.* 279:527–533.

Münchow, S., C. Sauter, and R.-P. Jansen. 1999. Association of the class V myosin Myo4p with a localised messenger RNA in budding yeast depends on She proteins. *J. Cell Sci.* 112:1511–1518.

Munro, T.P., R.J. Magee, G.J. Kidd, J.H. Carson, E. Barbarese, L.M. Smith, and R. Smith. 1999. Mutational analysis of a heterogeneous nuclear ribonucleoprotein A2 response element for RNA trafficking. *J. Biol. Chem.* 274: 34389–34395.

Norvell, A., R.L. Kelley, K. Wehr, and T. Schüpbach. 1999. Specific isoforms of Squid, a *Drosophila* hnRNP, perform distinct roles in Gurken localization during oogenesis. *Genes Dev.* 13:864–876.

Provance, D.W., Jr., and J.A. Mercer. 1999. Myosin-V: head to tail. *Cell. Mol. Life Sci.* 56:233–242.

Pruyne, D.W., D.H. Schott, and A. Bretscher. 1998. Tropomyosin-containing actin cables direct the Myo2p-dependent polarized delivery of secretory vesicles in budding yeast. *J. Cell Biol.* 143:1931–1945.

Reck-Peterson, S., P.J. Novick, and M.S. Mooseker. 1999. The tail of a yeast class V myosin, Myo2p, functions as a localization domain. *Mol. Biol. Cell.* 10: 1001–1017.

Reck-Peterson, S.L., D.W. Provance, Jr., M.S. Mooseker, and J.A. Merser. 2000. Class V myosins. *Biochim. Biophys. Acta.* 1496:36–51.

Reck-Peterson, S.L., M.J. Tyska, P.J. Novick, and M.S. Mooseker. 2001. The yeast class V myosins, Myo2p and Myo4p, are nonprocessive actin-based motors. *J. Cell Biol.* 153:1121–1126.

Reilein, A.R., S.L. Rogers, M.C. Tuma, and V.I. Gelfand. 2001. Regulation of molecular motor proteins. *Int. Rev. Cytol.* 204:179–238.

Rossanese, O.W., C.A. Reinke, B.J. Bevis, A.T. Hammond, I.B. Sears, J. O'Connor, and B. Glick. 2001. A role for actin, Cdc1p, and Myo2p in the inheritance of late Golgi elements in *Saccharomyces cerevisiae*. *J. Cell Biol.* 153:47–61.

Schott, D., J. Ho, D. Pruyne, and A. Bretscher. 1999. The COOH-terminal domain of Myo2p, a yeast myosin V, has a direct role in secretory vesicle targeting. *J. Cell Biol.* 147:791–807.

Schott, D.H., R.N. Collins, and A. Bretscher. 2002. Secretory vesicle transport velocity in living cells depends on the myosin-V lever arm length. *J. Cell Biol.* 156:35–39.

Segref, A., K. Sharma, V. Doye, A. Hellwig, J. Huber, R. Lührmann, and E. Hurt. 1997. Mex67p, a novel factor for nuclear mRNA export, binds to both poly(A)+ RNA and nuclear pores. *EMBO J.* 16:3256–3271.

Setou, M., D.-H. Seog, Y. Tanaka, Y. Kanai, Y. Takei, M. Kawagishi, and N. Hirokawa. 2002. Glutamate-receptor-interacting protein GRIP1 directly steers kinesin to dendrites. *Nature.* 417:83–87.

Shyu, A.-B., and M.F. Wilkinson. 2000. The double lives of shuttling mRNA binding poteins. *Cell.* 102:135–138.

Sil, A., and I. Herskowitz. 1996. Identification of an asymmetrically localized determinant, Ash1p, required for lineage-specific transcription of the yeast HO gene. *Cell.* 84:711–722.

Takizawa, P.A., and R.D. Vale. 2000. The myosin motor, Myo4p, binds Ash1 mRNA via the adapter protein, She3p. *Proc. Natl. Acad. Sci. USA.* 97:5273–5278.

Takizawa, P.A., A. Sil, J.R. Swedlow, I. Herskowitz, and R.D. Vale. 1997. Actin-dependent localization of an RNA encoding a cell-fate determinant in yeast. *Nature.* 389:90–93.

Takizawa, P.A., J.L. DeRisi, J.E. Wilhelm, and R.D. Vale. 2000. Plasma membrane compartmentalization in yeast by messenger RNA transport and a septin diffusion barrier. *Science.* 290:341–344.

Tanaka, H., K. Homma, A.H. Iwane, E. Katayama, R. Ikebe, J. Saito, T. Yanagida, and M. Ikebe. 2002. The motor domain determines the large step of myosin-V. *Nature.* 415:192–195.

Titus, M.A., and S.P. Gilbert. 1999. The diversity of molecular motors: an overview. *Cell. Mol. Life Sci.* 56:181–183.

Wach, A., A. Brachat, C. Alberti-Segui, C. Rebischung, and P. Phillippsen. 1997. Heterologous *HIS3* marker and GFP reporter modules for PCR-targetting in *Saccharomyces cerevisiae*. *Yeast.* 13:1065–1075.

Yin, H., E.D. Pruyne, T.C. Huffaker, and A. Bretscher. 2000. Myosin V orientates the mitotic spindle in yeast. *Nature.* 406:1013–1025.